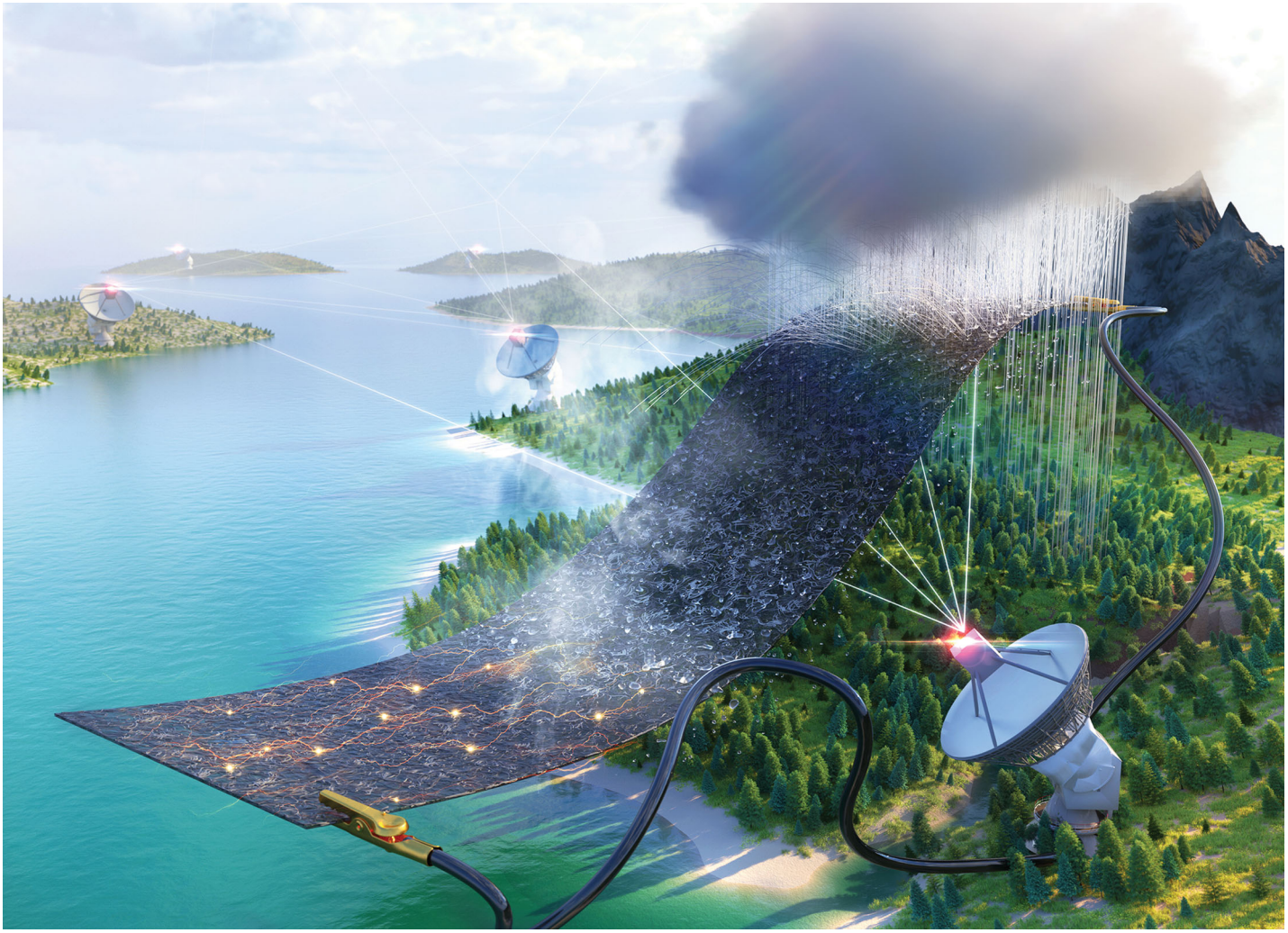

Showcasing research from Professor Il-Doo Kim's laboratory, Department of Materials Science and Engineering, Korea Advanced Institute of Science and Technology, Daejeon, Republic of Korea.

Self-operating transpiration-driven electrokinetic power generator with an artificial hydrological cycle

Water-powered generators have gained great attention since water is one of the most abundant renewable resources in nature. However, the generators need a periodical supply of water for continuous operation. Here, Il-Doo Kim *et al.* built an artificial hydrological cycle by using deliquescent calcium chloride to continuously supply water to self-operating transpiration-driven electrokinetic power generators (STEPGs); as the natural hydrological cycle provides water to forests. The developed STEPG could directly light a light-emitting diode and charge a supercapacitor for a week, which shows its huge potential as an energy source for low-power electronics and IoT technologies.

As featured in:

See Il-Doo Kim *et al.*, *Energy Environ. Sci.*, 2020, **13**, 527.

ROYAL SOCIETY OF CHEMISTRY

rsc.li/ees

Registered charity number: 207890

Energy & Environmental Science

ROYAL SOCIETY OF CHEMISTRY

PAPER

View Article Online
View Journal | View Issue

Cite this: *Energy Environ. Sci.*, 2020, **13**, 527

Self-operating transpiration-driven electrokinetic power generator with an artificial hydrological cycle†

Jaehyeong Bae, ‡[a] Tae Gwang Yun,‡[a] Bong Lim Suh, [b] Jihan Kim [b] and Il-Doo Kim *[a]

Autonomous energy scavenging from the ambient environment, or self-energy management, has attracted increasing attention because it could solve the energy problem of abundant Internet of things (IoT) devices. In recent years, several energy harvesters that generate electricity using water have been invented due to their simplicity, sustainability, and eco-friendliness. Until now, the devices have required periodic supplementation of water for continuous electricity generation, which hinders their practical use. Here, we built an artificial hydrological cycle in a transpiration-driven electrokinetic power generator (TEPG) to continuously and autonomously generate electric power. The TEPG, composed of carbon-coated cotton fabric, generates electricity by using a few drops of water (0.2 mL); the electric power originates from the potential difference in the asymmetrically wetted device and the pseudostreaming current. However, after only one hour, the TEPG stops generating electricity, as water inevitably evaporates from the device. For continuous self-operation, we utilized calcium chloride ($CaCl_2$), a typical deliquescent chemical, to collect water vapor from the surrounding environment and continuously supply water to the TEPG. In the range of 15–60% relative humidity (RH), $CaCl_2$ successfully compensates for the water loss by evaporation and maintains the electrical power generation in the closed system. In addition, $CaCl_2$ enhances the generated voltage (0.74 V) and current (22.5 μA) by supplying additional Ca^{2+} ions to the carbon surface and reducing the resistance of the device, respectively. The developed self-operating transpiration-driven electrokinetic power generator (STEPG) is stable enough to light a light-emitting diode (LED) for a week and charge a commercialized supercapacitor (5 F) to 1.6 V for 8 days.

Received 14th August 2019,
Accepted 22nd November 2019

DOI: 10.1039/c9ee02616a

rsc.li/ees

Broader context

Water is one of the most abundant renewable resources in nature. Due to its sustainability and eco-friendliness, numerous electricity generation technologies that utilize water as an energy source have emerged in recent years. However, like any other generators, water-powered generators need a periodical supply of water since it evaporates from the devices, which hinders their utility. Here, we built an artificial hydrological cycle by using deliquescent calcium chloride to continuously supply water to self-operating transpiration-driven electrokinetic power generators (STEPGs), as the natural hydrological cycle supplies water to the forest. The developed STEPG could directly light a light-emitting diode and charge a supercapacitor for a week, which shows its huge potential as an energy source for low-power electronics and IoT technologies.

Introduction

In recent years, energy harvesting devices that utilize water as an energy source have gained great attention since water is the most abundant and ubiquitous liquid on earth.[1–3] A variety of devices have been reported, where each device requires their own methods for water supplementation.[1–6] For example, Liang, *et al.* demonstrated a graphene oxide (GO) paper-based moisture-driven electric power generator,[5] and Xu *et al.* presented a pristine GO film-based water diffusion-driven power generator.[6] Unfortunately, all of these methods could only enable electricity generation over a short period since water naturally evaporates from the devices, terminating the generation of electricity. Therefore, a water-based energy harvester requires continuous or periodic water supply unless the device is installed at a large water source, such as a lake, a river, or an ocean. Nonetheless, these devices (maximum power of less than 1 mW) are highly suitable as an energy source for the vast

[a] *Department of Materials Science and Engineering, Korea Advanced Institute of Science and Technology (KAIST), 291 Daehak-ro, Yuseong-gu, Daejeon, 34141, Republic of Korea. E-mail: idkim@kaist.ac.kr*
[b] *Department of Chemical and Biomolecular Engineering, Korea Advanced Institute of Science and Technology (KAIST), 291 Daehak-ro, Yuseong-gu, Daejeon, 34141, Republic of Korea*

† Electronic supplementary information (ESI) available. See DOI: 10.1039/c9ee02616a

‡ These authors contributed equally to this work.

number of Internet of things (IoT) devices placed in various locations.[7,8] Desirably, the allocation of these devices should not be restricted by place, and a continuous water supply should be guaranteed for their practical use.

Many scientists have learned from nature and have adopted the knowledge from nature to solve scientific and engineering problems.[9,10] A transpiration-driven electrokinetic power generator (TEPG) is a good example of adopting the process of transpiration in plants to build a water-based energy harvester.[11] In nature, plants uptake essential nutrients through the transpiration process, which drives water from the roots and leaves (Fig. 1a).[12–15] During the process, water travels through the veins, driven by capillary action. A TEPG, composed of carbon-coated cotton fabric, utilizes a similar process to drive energy generation. For the operation of the TEPG, a small amount of water should be dropped on the negative electrode side to form an asymmetrically wetted carbon-coated cotton fabric (Fig. 1a).[11] At the interface between wet and dry carbon, the water content gradient drives continuous capillary flow of water from the wet to dry side. This capillary action on the conductive carbon surface induces a unique electrokinetic charge transfer through the carbon networks, called a pseudostreaming current (Fig. 1b). The main difference between a conventional streaming current and a pseudostreaming current lies in the conductivity of the channel for the water stream; the conventional streaming current corresponds to the current through liquids, whereas the pseudostreaming current corresponds to the current through conducting channels.[16] A potential difference originates from the electrical double layer on the wetted carbon surface compared with the dry carbon. Therefore, the presence of water maintaining the wetting asymmetry of the device is crucial for power generation in the TEPG. However, applied water eventually evaporates from the device, which limits continuous energy generation, similar to the aforementioned water-based energy harvesters. To overcome this limitation, water should be repeatedly applied to the TEPG, or the TEPG should somehow collect water from the environment by itself.

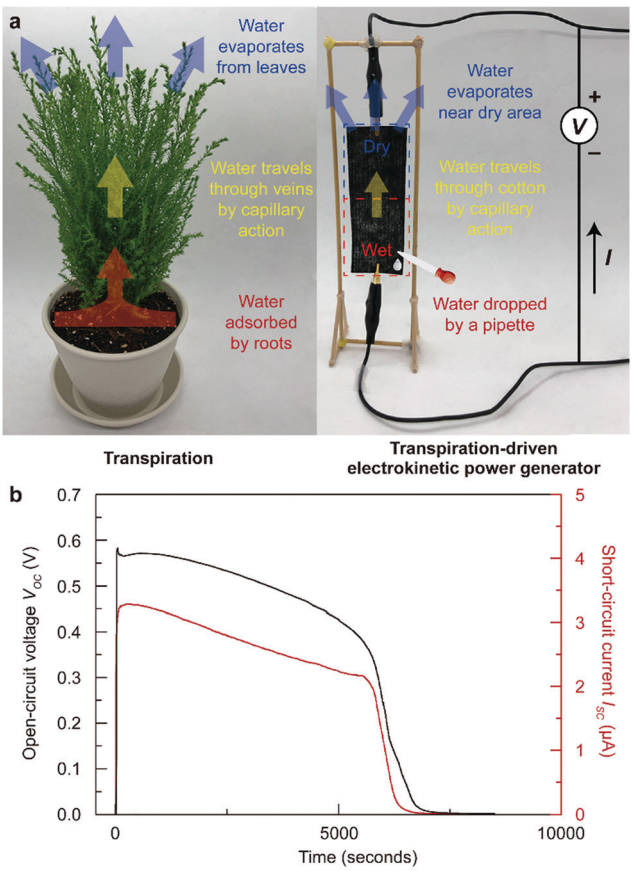

Fig. 1 TEPG. (a) Transpiration of plants (left) and the electrokinetic power generator whose operation resembles the transpiration of plants (right). (b) Measured V_{OC} and I_{SC} from the 120 kΩ TEPG generated by dropping 0.25 mL of DI water.

Water is indispensable for plants and is predominantly supplied through a process called the hydrological cycle.[17–20] The primary hydrological cycle is composed of evaporation of oceans, precipitation in clouds and ground surface runoff.[21,22] In addition, plants are involved in a subset of the hydrological cycle through the evapotranspiration process, by which plants uptake water from soil and vaporize it into the air through their roots and leaves.[23,24] If a water-based energy harvester could adopt a hydrological cycle with the near environment similar to how plants acquire a stable water supply through the evapotranspiration process, then the management of the water supply for the harvester would be independent, realizing autonomous energy harvesting.

Here, we incorporated $CaCl_2$ into a TEPG system to mimic the natural hydrological cycle to provide an autonomous supply of water to the TEPG (Fig. 2a). Calcium chloride, the main ingredient of desiccants, absorbs moisture from the surrounding air to form a saturated solution (Fig. 2b).[25,26] By dropping a $CaCl_2$ solution on the TEPG, we successfully eliminated repeated human work for continuous energy harvesting, *i.e.*, a self-operating transpiration-driven electrokinetic power generator (STEPG; Fig. 2c) was realized. Since the deliquescence has a close relationship with the humidity, we systematically studied the power generation efficiency of the STEPG by varying the amount of $CaCl_2$ and humidity level. The enhanced electrical power of the STEPG upon the addition of $CaCl_2$ was verified by density functional theory (DFT) calculations and modeling of the electric circuit. Our simple and environmentally friendly approach could be easily applicable to other water-based energy harvesters and many other fields that require acquiring water in a self-driven way.

Experimental section

Fabrication and characterization of a self-operating transpiration-driven electrokinetic power generator (STEPG)

For the fabrication of the STEPG, 0.2 g of Ketjen black powder (Lion Specialty Chemicals Co., Ltd, ec600jd model) was dispersed in DI water (40 mL) with 0.4 g of cetrimonium bromide (CTAB, Sigma Aldrich) surfactant. For uniform dispersion of the Ketjen black, the solution was sonicated for 1 hour. Then, cotton fabric (3 cm × 9 cm × 0.12 mm) was dip-coated in the Ketjen black ink, and the Ketjen black-coated cotton fabric was dried in an oven at 80 °C for 30 min. STEPGs with resistances ranging from a few kΩ to tens of MΩ were prepared by controlling the mass loading of

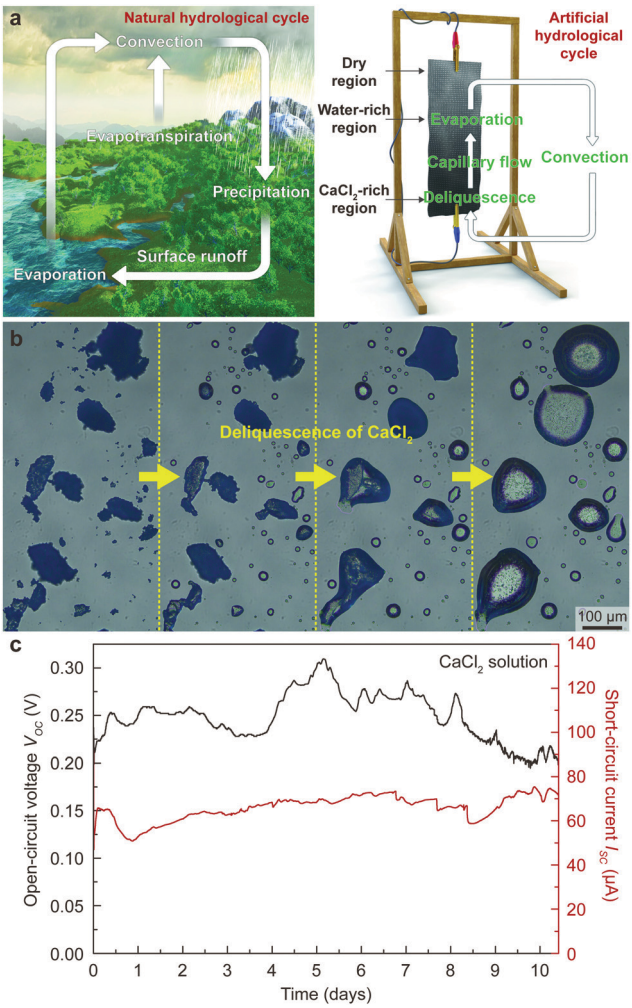

Fig. 2 Artificial hydrological cycle system for the STEPG. (a) Schematic illustration of natural hydrological cycle and artificial hydrological cycle for the STEPG. (b) Optical microscope image of $CaCl_2$ exposed to 40% RH, showing typical deliquescent behavior. (c) Continuous V_{OC} and I_{SC} generated by applying 0.25 mL of saturated $CaCl_2$ solution onto a stacked carbon black-coated cotton fabric (base resistance: 5 kΩ) at 25 °C and 35% RH.

Ketjen black by varying the concentration of the ink and/or the number of times the fabric was dipped into the ink. The open-circuit voltage (V_{OC}) and short-circuit current (I_{SC}) of the STEPGs were measured by an electrometer (6517A, Keithley). For operation, saturated $CaCl_2$ solution was gently applied on Ketjen black-coated cotton fabric. We installed the STEPGs in a vertical manner with the wetted area at the bottom to manage capillary action by gravity. The humidity of the closed environment was controlled by a humidifier (OA-HM250, K2C International Co.). After stabilization of humidity for 6 hours, humidity and temperature were measured by a digital thermos-hygrometer (TT-580, Tanita).

Application of STEPGs in lighting a light-emitting diode (LED), charging a supercapacitor

A red LED, YINHUI Photoelectric, with a drive voltage of 2.2 V and a drive current of 20 mA, was powered by a 15 series connection of 3 stacked STEPGs without a rectifier circuit (Fig. 5b). In addition, the electricity generated from the STEPGs (15 series connection of 3 stacked STEPGs) was stored in five commercialized supercapacitors (SAMXON, 1 F capacitance) without a rectifier component (Fig. 5c). The supercapacitor was charged up to 1.6 V for 8 days.

Charge redistribution DFT calculations

First-principles calculations were performed with the Vienna *ab initio* simulation program (VASP)[27] based on the plane-wave basis set to describe the charge transfer behavior of calcium cations on the carbon surface. Since the surface of Ketjen black is easily oxidized upon air exposure, we used oxygen-functionalized graphene for the simulation study. The projected-augmented wave (PAW)[28] method was used to describe the electron–ion interactions, and for valence electrons, a plane-wave basis set was employed. The generalized gradient approximation method known as GGA-PBE[29] was used for the exchange–correlation functional. A cut-off energy of 500 eV was imposed for the plane-wave basis set, and Γ-point sampling was used for the Brillouin zone integration. To nullify the interactions between periodic images along the axis perpendicular to the surface, all slabs were separated by 20 Å along this direction perpendicular. The initial structures were generated by Materials Studio,[30] and the initial geometries were further relaxed *via* DFT simulations. To quantify the charge transfer properties between the cation and the graphene, charge partitioning was calculated with the Bader[31] method as implemented in VASP[27] and provided by the BADER tool.[32]

Results and discussion

Autonomous and continuous energy generation of the STEPG by using $CaCl_2$

Calcium chloride on the STEPG plays a pivotal role in forming an artificial hydrological cycle, which has the following three steps. (1) The $CaCl_2$ region on the STEPG collects moisture from the air through deliquescence. (2) The dry region wicks water *via* the cotton fabric from the $CaCl_2$ region, forming a water-wetted region. (3) Water evaporates from the water-wetted region into the air (Fig. 2a). After single dropping of $CaCl_2$ solution, the STEPG maintains stable wetting asymmetry and spontaneously generates power through artificial hydrological circulation (Fig. 2c). The natural hydrological cycle process inevitably has intervals because rain only falls when the criteria for precipitation in clouds are satisfied. In contrast, the criteria for evaporation, diffusion, and deliquescence on the STEPG are satisfied across a broad range of temperatures and humidities, including at ambient conditions; therefore, the artificial hydrological cycle occurs all the time in lab conditions.

Effect of $CaCl_2$ content on energy generation of the STEPG

Because wetting asymmetry of the STEPG is key for energy generation, finding a suitable amount of $CaCl_2$ to maintain the appropriate ratio of wet and dry regions is critical. The STEPG was installed vertically to manage the capillary flow driven by the gravity force. If too little $CaCl_2$ is applied on the device,

evaporation will dominate the deliquescence, reducing the wet area and thus abating the power generation. If the applied $CaCl_2$ is too much, deliquescence will overwhelm evaporation, and the entire device will be wetted, thus terminating the energy generation. $CaCl_2$ was applied to the STEPG in the form of solution by dissolving it in DI water; therefore, we controlled the optimal amount of $CaCl_2$ by varying the concentration of the solution. As long as the dropped solution contained $CaCl_2$, the STEPG produced continuous V_{OC} and I_{SC} (Fig. 3a and Fig. S1, ESI†). The $CaCl_2$ concentration affects the generated voltage and current values because it determines the quality of the electrical double layer formed at the solution/carbon interface and the resistance of the liquid as well as the device. In ambient conditions, both dilute and supersaturated $CaCl_2$ solutions gradually become saturated solutions, eventually forming a thermodynamic equilibrium. Water in the dilute $CaCl_2$ solution evaporates, and the amount of solution decreases. Below the concentration of 2.67 M, the voltage profile shows a steep decrease around 7000 s, which is the time for evaporation of water to saturate the solution. The large amount of Ca^{2+} ions in a high concentration $CaCl_2$ solution contributes to a higher charge density in the electrical double layer, resulting in increased V_{OC}, which will be discussed later. Above 2.67 M, the amount of $CaCl_2$ is large enough to develop a high and equal quality electrical double layer near the negative electrode (downside) due to the vertical setup of the STEPG; therefore, the measured V_{OC} values are similar over time without a steep decrease. Compared to V_{OC}, I_{SC} is not saturated even at high concentrations (Fig. S1, ESI†). This result shows that the origins of the voltage and current generation are distinct for TEPGs.[11] With a high concentration of $CaCl_2$, the wet region collects more water to facilitate capillary flow and generate a higher current based on pseudostreaming theory. In addition to the enhanced capillary flow, the internal resistance of the device also affects the I_{SC} value, which will be discussed later along with Fig. 4a. A high concentration salt solution exhibits lower resistance than DI water. Therefore, the resistance of the working STEPG operated by $CaCl_2$ solution is lower than that of the TEPG operated by DI water. The lower internal resistance is attributed to the lower resistive loss during energy generation, which results in higher I_{SC} (Fig. S2a, ESI†). In addition to the above reasons, the use of saturated $CaCl_2$ solution is desirable for precise control of the wet and dry areas to maintain the wetting asymmetry of the device.

Humidity effect on energy generation of the STEPG

The deliquescent property of $CaCl_2$ is mainly governed by the humidity (Fig. 3b and Fig. S3, ESI†). Under 20% relative humidity (RH) at room temperature, $CaCl_2$ exists in crystalline hydrate form.[25] In this condition, no water molecules and solvated ions can be provided to the carbon surface for building the surface charge density; therefore, the STEPG does not generate V_{OC} and I_{SC}. Above 20% RH, $CaCl_2$ collects water from the environment and supplies water to the STEPG, leading to stable V_{OC} and I_{SC}. At a humidity over 60% RH, the whole STEPG is fully wetted by excessive water collection of $CaCl_2$. For the TEPG, loss of the wetting asymmetry results in no more power generation (Fig. 3c and Fig. S4, ESI†).[11] The fully wetted STEPG, however, interestingly

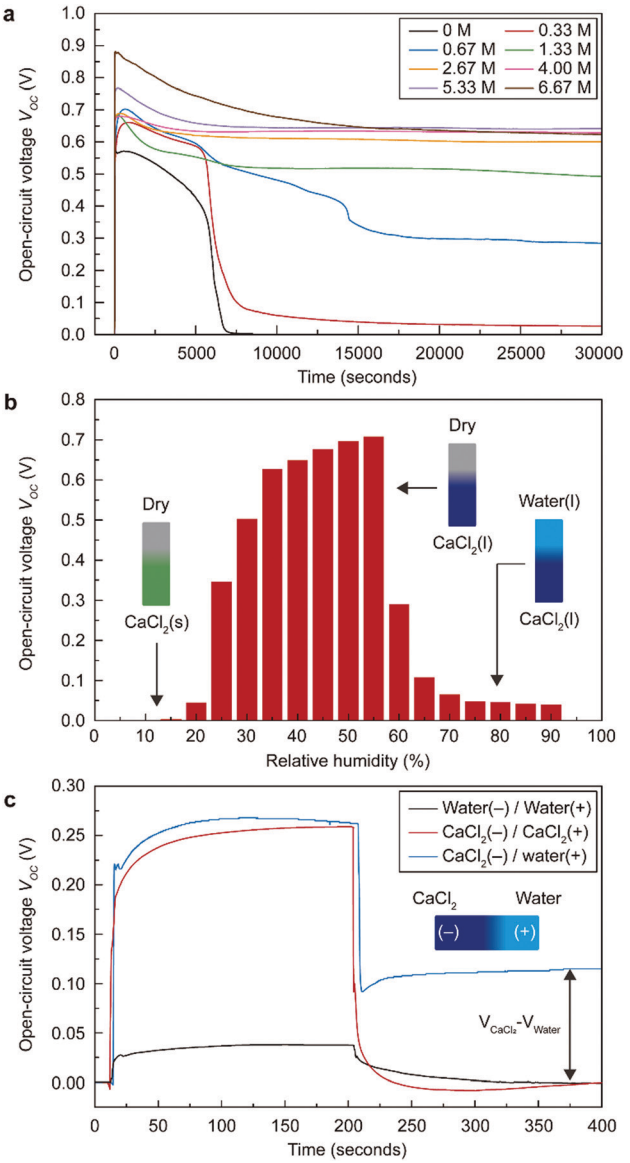

Fig. 3 Moisture-absorbing behavior of the STEPG. (a) Measured V_{OC} profiles generated by dropping various concentrations of $CaCl_2$ solution onto the STEPG (120 kΩ) at 26 °C and 40% RH. (b) Measured V_{OC} values of the STEPG (120 kΩ) at various RH conditions and 22 °C. (c) Measured V_{OC} values of the STEPG generated by dropping various combinations of DI water and saturated $CaCl_2$ solution onto the (–) and (+) electrodes. At first, a solution was added on the (–) electrode and at 200 s the other solution was applied on the (+) electrode.

generates V_{OC} and I_{SC}. The vertical setup limits the diffusion of calcium chloride to the positive (upper) electrode by gravity, so the solutions near the positive electrode and negative (lower) electrode have different $CaCl_2$ contents. In this situation, the potential difference comes from the different surface charge densities between the Ca^{2+}-free positive electrode and the Ca^{2+}-abundant negative electrode.

Similarly, the fully wetted STEPG at a humidity over 60% RH can generate a stable current (Fig. S3, ESI†). Although the device is fully wetted, the amount of water on the negative electrode side is greater than that on the positive electrode due

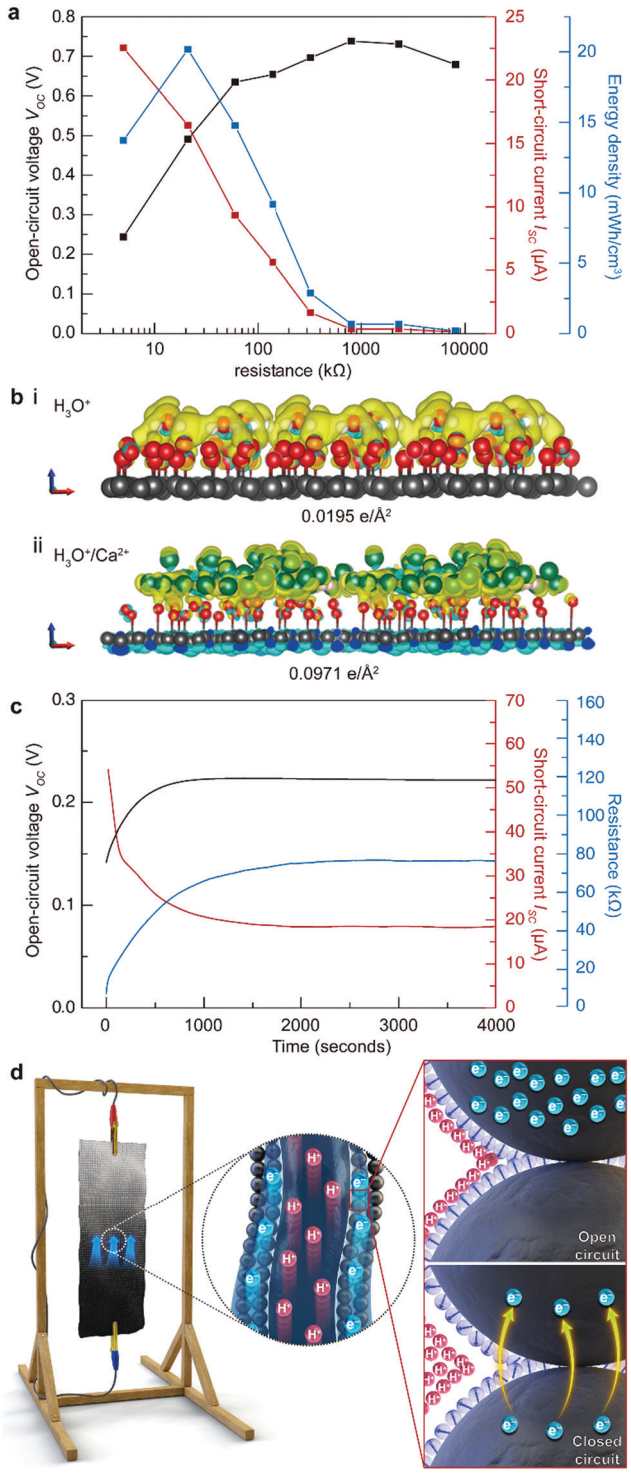

Fig. 4 Effect of resistance and Ca^{2+} ions on the energy generation of the STEPG. (a) Measured V_{OC}, I_{SC} and energy density values of various resistance STEPGs at 26 °C and 37% RH. (b) Charge redistribution on oxidized graphene covered by hydronium ions (i) and hydronium ions with calcium ions (ii) (yellow, losing an electron; blue, gaining an electron). The value of the electron redistribution on the carbon is located below each panel. (c) Measured V_{OC}, I_{SC}, and resistance profiles after stabilization for 3 hours to reduce the water content and resistance change. (d) Schematic illustration of dielectric scattering on the working STEPG and equivalent electric circuit. Blue balls containing arrows represent water molecules along with their polarity (dielectric field) in the inset.

to the continuous collection of water from the environment, generating a water content difference. In addition to water molecules, abundant Ca^{2+} ions on the negative electrode side diffuse to the positive electrode side due to the ion concentration gradient. This combination of two gradients, *i.e.*, protons and Ca^{2+} ions, contributes to the measured I_{SC}.

Energy generation in a high humidity environment (fully wetted STEPG with $CaCl_2$ content asymmetry)

To further investigate energy generation in the situation of $CaCl_2$ asymmetry in high humidity conditions, we dropped various combinations of DI water and saturated $CaCl_2$ solution at the negative and positive electrodes (Fig. 3c and Fig. S4, ESI†). When both the negative and positive electrodes are wetted by the same type of liquid, the generated V_{OC} converges to 0 even when the liquids are dropped in different orders. When the negative and positive electrodes are wetted by $CaCl_2$ solution and water, respectively, the STEPG produces a reduced V_{OC} (Table 1). The persistent V_{OC} is attributed to the potential difference between the carbons wetted by saturated $CaCl_2$ solution and DI water ($V_{OC,CaCl_2}$–$V_{OC,water}$). The value seems not to match the V_{OC} measured in the wet/dry situation; however, considering that V_{OC} changes with the internal resistance, the persistent voltage matches well with the voltage difference in terms of the potential difference due to the electrical double layer (V_{EDL} or $V_{EDL,CaCl_2}$–$V_{EDL,water}$) calculated by the equation below (Table 1, Table S1 and eqn (1); details in ESI†).

$$V_{OC} = \frac{\left(V_{EDL,CaCl_2} - V_{EDL,water}\right) R_{i,water}}{R_{i,CaCl_2} + R_{i,water}} \quad (1)$$

For the pseudostreaming current (I_{PST}), the measured I_{SC} profile has a similar trend as V_{OC} (Fig. S4, ESI†). From the calculation based on the analyzed electrical circuit (Fig. S2b, ESI†), we found that the I_{PST} at high humidity (fully wetted configuration with $CaCl_2$ asymmetry) is lower than that of the STEPG under ambient humidity and higher than that in the TEPG setting (Table S1 and eqn (2), details in ESI†).[11]

$$I_{SC} = \frac{I_{PST,CaCl_2} - I_{PST,water}}{1 + \dfrac{R_{w,CaCl_2} - R_{w,water}}{R_{i,water}}} \quad (2)$$

Based on pseudostreaming theory, I_{PST} should have the following proportionality.

$$I_{PST} \propto Q\sigma d \quad (3)$$

Table 1 Measured V_{OC} and calculated V_{EDL} or $V_{EDL,CaCl_2}$–$V_{EDL,water}$ generated by dropping DI water or saturated $CaCl_2$ solution on the (−) electrode or dropping saturated $CaCl_2$ solution and water on the (−) and (+) electrodes, respectively

Carbon black-coated cotton fabric (7.4 kΩ)	V_{OC} or $V_{OC,CaCl_2}$–$V_{OC,water}$ (V)	V_{EDL} or $V_{EDL,CaCl_2}$–$V_{EDL,water}$ (V)
(1) $CaCl_2$ (−)/dry (+)	0.259	0.336
(2) Water (−)/dry (+)	0.038	0.190
(3) $CaCl_2$ (−)/water (+)	0.115	0.123
(1)–(2)–(3)	0.106	0.023

where I_{PST} is the pseudostreaming current, Q is the flow rate, σ is the surface charge density, and d is the separation.

Compared with the STEPG under ambient humidity, the reduced I_{SC} at high humidity indicates that diminished flow occurs from the interface of the $CaCl_2$ rich regions to that of the $CaCl_2$ poor regions. In addition, the I_{PST} under $CaCl_2$ asymmetry is higher than that in the normal TEPG setting, showing that even though the flow rate is diminished, the diffusion of the surface charges (Ca^{2+}) largely enhances I_{PST}.

Evaluation of energy generated by the STEPG

Compared to the TEPG, the STEPG exhibits enhanced maximum V_{OC} (0.74 V), I_{SC} (22.5 μA) and electric power (2.02 μW), exhibiting superior energy performance over other water-based electricity generators (Fig. 4a, Fig. S5, S6 and Table S2, ESI†).[11] To verify the origin of the enhanced V_{OC} with Ca^{2+} ions, we calculated the surface charge density in the double layer caused by adsorption of water molecules and water molecules with Ca^{2+} ions on oxygen-functionalized graphene by DFT calculation (details in the Experimental section). When oxygen-functionalized graphene is covered only by water, a double layer forms at the water/graphene interface with a surface charge density of 0.0195 e $Å^{-2}$ on the graphene layer (Fig. 4b-i). In comparison, the surface charge density increases to 0.0971 e $Å^{-2}$ when Ca^{2+} ions are included in the solution (Fig. 4b-ii). The Ca^{2+} ions form an additional charge at the outer Helmholtz layer, thus increasing the overall surface charge density at graphene and hence increasing V_{EDL} as well as the measured V_{OC} (Fig. 4b).[33,34] In addition to the voltage, the conductivity of the solution would be increased by adding a salt, which minimizes the resistive loss during the operation of the STEPG and enhances the measured I_{SC} (for details, see ESI†).[35,36] Combining the above enhancement with a stable water supply, the STEPG exhibits an energy density of 22.4 mW h cm^{-3}. Moreover, reducing the size of the device can further enhance the energy density up to 135.6 mW h cm^{-3}, which is approximately 120-folds higher than that of the water-driven TEPG without Ca^{2+} addition (Fig. S7, ESI†).

Electrical double layer scattering phenomena due to a flood of electrons at the beginning of STEPG operation

As the STEPG could fix the water content gradient through the artificial hydrological cycle, we were able to find interesting physical phenomena at the beginning of the STEPG operation. At the initial stage (before 1000 s in Fig. 4c), V_{OC} and the resistance increase and I_{SC} decreases. In open-circuit conditions, the electrical double layer is well arranged on the carbon surface, as are the water molecules (dielectric fields) (Fig. 4d with the upper inset). When the STEPG forms a closed circuit, electrons start to flow through the carbons and the surrounding double layer (Fig. 4d under inset, for details of electron transfer, see ESI†). This electron flow disrupts ordered adsorbed protons and water molecules, which increases the Debye length of protons and the permittivity of the solution in the double layer.[37,38] The increase of V_{OC} and the internal resistance in the initial operation is attributed to a combination of the two effects.

Of course, an increase in the internal resistance should reduce I_{SC}. However, the pseudostreaming current on the STEPG enables the accumulation of electrons at the wet/dry interface even in open-circuit conditions (Fig. 4d upper inset). The accumulated electrons flood toward the positive electrode side after the closed-circuit connection, which leads to a 3-fold larger current than the stabilized values after 1000 s (Fig. 4c). This double layer scattering phenomenon at the beginning of STEPG operation would be obscured without the stable artificial hydrological cycle that maintains the water content at each electrode.

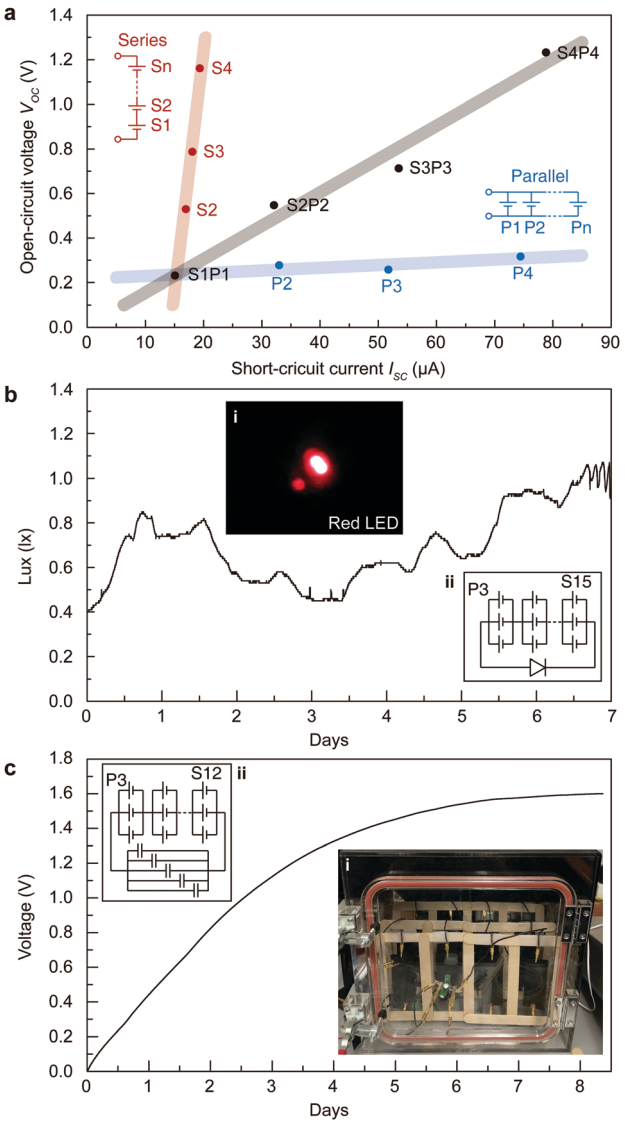

Fig. 5 Scaling up and long-term demonstration of STEPGs. (a) Enhanced V_{OC} and/or I_{SC} obtained by connecting multiple STEPGs in series and/or parallel (stacking method) connection. S stands for series connection, P stands for parallel connection and SxPy stands for x number of series connection of y number of parallel connection STEPGs. The R-square values of the red, black, and blue fitting lines are 0.86, 0.98, and 0.97, respectively. (b) Measured illuminance of a red LED powered by a 15 series connection of 3 stacked STEPGs for a week at 22–26 °C and 30–35% RH. Inset i, a photographic image of the red LED powered by STEPGs. Inset ii, the equivalent electric circuit. (c) Voltage profile of charging of 5 commercialized supercapacitors (5 F) by using a 12 series connection of 3 stacked STEPGs for 8 days at 22–26 °C and 30–35% RH. Inset i, a photographic image of the supercapacitors charged by STEPGs. Inset ii, the equivalent electric circuit.

Scaling up and demonstration of STEPG

The energy acquired from STEPGs can be scaled up by series and parallel (stacking manner) connection of STEPGs (Fig. 5a). The series connection of STEPGs multiplies the measured voltage, and the parallel connection multiplies the measured current in proportion to the number of connected STEPGs. The combination of series and parallel connections enlarges the measured voltage and current at the same time without any loss. This simple scaling allows us to design the connection of multiple STEPGs to run a device that has arbitrary voltage and current requirements. To emphasize the long-term energy generation, we successfully lighted a red LED (0.65 lux on average) for a week by using a 15 series connection of 3 stacked STEPGs without any additional elements (Fig. 5b). In addition, the generated power is capable of charging a commercialized supercapacitor (5 F) up to 1.6 V for 8 days using a 12 series connection of 3 stacked STEPGs (Fig. 5c).

Conclusions

We successfully elongated the energy generation time of the STEPG through autonomous operation *via* incorporation of $CaCl_2$ to establish an artificial hydrological cycle. Although the STEPG can operate above 20% RH, the optimum humidity range is 30–55% RH considering the electric power. In addition, the STEPG exhibits enhanced power and energy density 120-fold higher than those of the water-driven TEPG due to the enhanced surface charge density arising from Ca^{2+} ions and the conductivity of the device. In addition, systematic analysis revealed electrical double layer scattering phenomena at the beginning of operation. The excellent scalability with practical demonstrations verifies the feasibility of using the STEPG as an energy source. Adopting nature's ubiquity and sustainability, the STEPG clearly demonstrates a novel way to improve the utility of energy harvesters, making it highly suitable for large networks of low-power IoT devices.

Conflicts of interest

There are no conflicts to declare.

Acknowledgements

This work was supported by the Samsung Research Funding & Incubation Center of Samsung Electronics under Project Number SRFC-MA1802-05.

Notes and references

1 W. Olthuis, B. Schippers, J. Eijkel and A. Van Den Berg, *Sens. Actuators, B*, 2005, **111–112**, 385–389.
2 T. Nguyen, Y. Xie, L. J. de Vreede, A. van den Berg and J. C. T. Eijkel, *Lab Chip*, 2013, **13**, 3210–3216.
3 B. Fan, A. Bhattacharya and P. R. Bandaru, *Nat. Commun.*, 2018, **9**, 4050.
4 G. Xue, Y. Xu, T. Ding, J. Li, J. Yin, W. Fei, Y. Cao, J. Yu, L. Yuan, L. Gong, J. Chen, S. Deng, J. Zhou and W. Guo, *Nat. Nanotechnol.*, 2017, **12**, 317–321.
5 Y. Liang, F. Zhao, Z. Cheng, Y. Deng, Y. Xiao, H. Cheng, P. Zhang, Y. Huang, H. Shao and L. Qu, *Energy Environ. Sci.*, 2018, **11**, 1730–1735.
6 T. Xu, X. Ding, C. Shao, L. Song, T. Lin, X. Gao, J. Xue, Z. Zhang and L. Qu, *Small*, 2018, **14**, 1704473.
7 R. Want, W. Wang and S. Chesnutt, *Computer*, 2018, **51**, 66–70.
8 X. Liu, Z. Qin, Y. Gao and J. A. McCann, *IEEE Internet Things J.*, 2019, **6**, 4935–4945.
9 B. Bhushan, *Philos. Trans. R. Soc., A*, 2009, **367**, 1445–1486.
10 G. D. Scholes, G. R. Fleming, A. Olaya-Castro and R. Van Grondelle, *Nat. Chem.*, 2011, **3**, 763–774.
11 T. G. Yun, J. Bae and I.-D. Kim, *ACS Nano*, 2019, **13**, 12703–12709.
12 R. K. Sinha, *Modern Plant Physiology*, Alpha Science International, Pangbourne, 2004.
13 L. Taiz, E. Zeiger, I. M. Moller and A. S. Murphy, *Plant Physiology and Development*, Oxford University Press, Sunderland, 2018.
14 S. Jasechko, Z. D. Sharp, J. J. Gibson, S. J. Birks, Y. Yi and P. J. Fawcett, *Nature*, 2013, **496**, 347–350.
15 J. Evaristo, S. Jasechko and J. J. McDonnell, *Nature*, 2015, **525**, 91–94.
16 A. V. Delgado, F. González-Caballero, R. J. Hunter, L. K. Koopal and J. Lyklema, *Pure Appl. Chem.*, 2005, **77**, 1753–1805.
17 M. T. Chahine, *Nature*, 1992, **359**, 373–380.
18 W. R. L. Anderegg, A. G. Konings, A. T. Trugman, K. Yu, D. R. Bowling, R. Gabbitas, D. S. Karp, S. Pacala, J. S. Sperry, B. N. Sulman and N. Zenes, *Nature*, 2018, **561**, 538–541.
19 T. Oki and S. Kanae, *Science*, 2006, **313**, 1068–1072.
20 P. Falkowski, R. J. Scholes, E. Boyle, J. Canadell, D. Canfield, J. Elser, N. Gruber, K. Hibbard, P. Högberg, S. Linder, F. T. Mackenzie, B. Moore III, T. Pedersen, Y. Rosenthal, S. Seitzinger, V. Smetacek and W. Steffen, *Science*, 2000, **290**, 291–296.
21 W. Brutsaert and M. B. Parlange, *Nature*, 1998, **396**, 30.
22 V. Ramanathan, P. J. Crutzen, J. T. Kiehl and D. Rosenfeld, *Science*, 2001, **294**, 2119–2124.
23 G. B. Bonan, *Science*, 2008, **320**, 1444–1449.
24 P. B. Reich, K. M. Sendall, A. Stefanski, R. L. Rich, S. E. Hobbie and R. A. Montgomery, *Nature*, 2018, **562**, 263–267.
25 R. V. Gough, V. F. Chevrier and M. A. Tolbert, *Planet. Space Sci.*, 2016, **131**, 79–87.
26 L. J. Mauer and L. S. Taylor, *Annu. Rev. Food Sci. Technol.*, 2010, **1**, 41–63.
27 G. Kresse and D. Joubert, *Phys. Rev. B: Condens. Matter Mater. Phys.*, 1999, **59**, 1758–1775.
28 P. E. Blöchl, *Phys. Rev. B: Condens. Matter Mater. Phys.*, 1994, **50**, 17953–17979.
29 J. P. Perdew, K. Burke and Y. Wang, *Phys. Rev. B: Condens. Matter Mater. Phys.*, 1996, **54**, 16533–16539.
30 Materials Studio, Accelrys. co.
31 R. F. W. Bader, *Chem. Rev.*, 1991, **91**, 893–928.
32 G. Henkelman, A. Arnaldsson and H. Jónsson, *Comput. Mater. Sci.*, 2006, **36**, 354–360.

33 P. B. Antin, S. Forry-Schaudies and T. M. Friedman, *J. Cell Biol.*, 1981, **91**, 99–110.
34 R. K. Kalluri, T. A. Ho, J. Biener, M. M. Biener and A. Striolo, *J. Phys. Chem. C*, 2013, **117**, 13609–13619.
35 A. V. Wolf, *Aqueous Solutions and Body Fluids*, New York, 1966.
36 R. C. Weast, *CRC Handbook of Chemistry and Physics*, CRC Press, Boca Raton, 70th edn, 1989.
37 H. Wang and L. Pilon, *J. Phys. Chem. C*, 2011, **115**, 16711–16719.
38 E. Gongadze, U. van Rienen and A. Iglič, *Cell. Mol. Biol. Lett.*, 2011, **16**, 576–594.